International Journal of High-Rise Buildings
March 2015, Vol 4, No 1, 9-25

International Journal of
High-Rise Buildings
www.ctbuh-korea.org/ijhrb/index.php

Field Measurement and Modal Identification of Various Structures for Structural Health Monitoring

Akihiko Yoshida[1,†] and Yukio Tamura[1,2]

[1]*Tokyo Polytechnic University*
[2]*School of Civil Engineering, Beijing Jiaotong University*

Abstract

Field measurements of various structures have been conducted for many purposes. Measurement data obtained by field measurement is very useful to determine vibration characteristics including dynamic characteristics such as the damping ratio, natural frequency, and mode shape of a structure. In addition, results of field measurements and modal identification can be used for modal updating of FEM analysis, for checking the efficiency of damping devices and so on. This paper shows some examples of field measurements and modal identification for structural health monitoring. As the first example, changes of dynamic characteristics of a 15-story office building in four construction stages from the foundation stage to completion are described. The dynamic characteristics of each construction stage were modeled as accurately as possible by FEM, and the stiffness of the main structural frame was evaluated and the FEM results were compared with measurements performed on non-load-bearing elements. Simple FEM modal updating was also applied. As the next example, full-scale measurements were also carried out on a high-rise chimney, and the efficiency of the tuned mass damper was investigated by using two kinds of modal identification techniques. Good correspondence was shown with vibration characteristics obtained by the 2DOF-RD technique and the Frequency Domain Decomposition method. As the last example, the wind-induced response using RTK-GPS and the feasibility of hybrid use of FEM analysis and RTK-GPS for confirming the integrity of structures during strong typhoons were shown. The member stresses obtained by hybrid use of FEM analysis and RTK-GPS were close to the member stresses measured by strain gauges.

Keywords: Field measurement, Damping ratio, System identification

1. Introduction

Field measurements of various structures have been conducted for many purposes. Measurement data obtained by field measurement is very useful to determine vibration characteristics including dynamic characteristics such as damping ratio, natural frequency, and mode shape of a structure. In addition, results of field measurement and modal identification can be used for modal updating of FEM analysis, for checking the efficiency of damping devices and so on. Dynamic characterization of civil engineering structures is becoming increasingly important for dynamic response prediction, finite element modal updating and structural health monitoring, as well as for passive and active vibration control of buildings, towers, long-span bridges, etc. The dynamic characteristics of a structure can be obtained by traditional experimental modal analysis. This requires artificial excitation and measurement of both responses and excitation forces. Many civil engineering structures can be adequately excited by ambient (natural) excitations such as wind, turbulence, traffic, and/or micro-seismic tremors. Ambient modal analysis based on response measurements has two major advantages compared to traditional analysis. One is that no expensive and heavy excitation devices are required. The other is that all (or part) of the measurements can be used as references, and multi-input multi-output techniques can be used for modal analysis, thus enabling easy handling of closely-spaced and even repeated modes.

On the other hand, accelerometers have been used for field measurements of wind-induced responses of buildings. However, wind-induced responses consist of a static component, i.e., a mean value, and a dynamic fluctuating component. The static component is difficult to measure with accelerometers. Çelebi[1] proposed the use of RTK-GPS for measurements of building responses. An RTK-GPS (Leica MC1000) has a nominal accuracy of ±1 cm +1 ppm for horizontal displacements and ±2 cm +2 ppm for vertical displacements with a sampling rate of 10Hz.[2] Considering the static component and the first mode predominance for wind-induced responses, GPS is better for wind-induced response measurements. According to the feasibility study of RTK-GPS for measuring wind-induced responses of buildings, responses with amplitudes larger

[†]Corresponding author: Akihito Yoshida
Tel: +81-46-242-9540; Fax: +81-46-242-9540
E-mail: yoshida@arch.t-kougei.ac.jp

than 2 cm and natural frequencies lower than 2 Hz can be detected by RTK-GPS.[3-5]

This paper shows some examples of field measurements and modal identification for structural health monitoring. As the first example, changes of dynamic characteristics of a 15-story office building in four construction stages from the foundation stage to completion are described. Ambient response measurements of the office building in the field at different construction stages were planned in order to investigate the variation of its dynamic characteristics during construction. This was done in order to examine the separate contributions of the steel frames, the column concrete, the floor slabs, the external walls, the internal walls, etc., to the building's dynamic characteristics. Detecting the change in the dynamic characteristics with the addition of structural members or architectural parts enabled more accurate quantitative evaluation of the contribution of these members and parts to the analytical finite element model (FEM) of the building. Simple FEM modal updating based on the dynamic characteristics obtained by the field measurement was also applied. Another research project on ambient response field measurements of a high-rise steel chimney is also reported, where the dynamic characteristics are obtained by frequency domain decomposition (FDD) and a newly proposed 2DOF-RD technique. In this field measurement, the efficiency of the tuned mass damper was investigated by using two kinds of modal identification techniques. Good correspondence was shown with vibration characteristics obtained by the 2DOF-RD technique and the FDD method. The other object of this paper is to demonstrate the efficiency of RTK-GPS in measuring the displacement of a full-scale tower and to study the feasibility of hybrid use of FEM analysis and RTK-GPS for detecting the integrity of structures during strong typhoons. The results of the other project for full scale measurement by RTK-GPS for high-rise office building is also introduced. The possibility of the measurement of seismic response by RTK-GPS was shown with the results of the 2011 off the Pacific coast of Tohoku Earthquake.

2. FEM Modal Update Based on Dynamic Characteristics by Field Measurement of 15-story Office Building[6,7]

2.1. Outline of Tested CFT building

The building tested is a middle-rise 15-story office building 53.4 m high, located in Ichigaya, Tokyo. It extends from 6.1 m underground to 59.15 m above basement level, as shown in Fig. 1. It has one story beneath ground level and 15 stories above. The columns are concrete-filled-tube (CFT), as shown in Fig. 2, and the beams are wide-flange steel. The floor comprises a concrete slab and steel deck. The exterior walls of the first floor are of pre-cast concrete. The walls from the second floor to the top are of autoclaved lightweight concrete (ALC). The ALC exterior

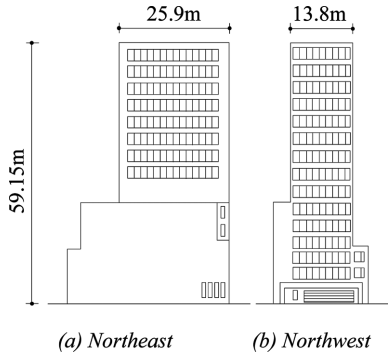


Figure 1. Elevation of 15-story office building.

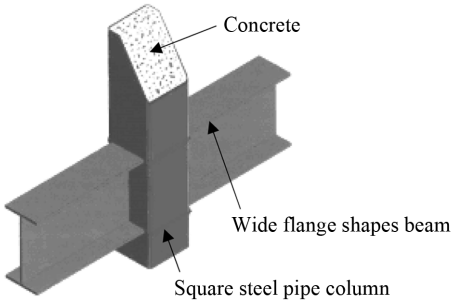


Figure 2. Concrete-Filled-Tube (CFT) column.

walls are attached by a half locking method. The interior walls are attached by the slide method. The plan of a standard story is 22.2 m long by 13.8 m wide, and the floor-to-floor height is 3.8 m. The piles are under the foundations, and the underground story is of SRC (steel-encased reinforced concrete). When the steel frame portion was erected up to the 11th floor, the CFT columns were filled with concrete. The concrete was placed by the pressing method from the first floor pedestal portion. After that, the steel frame was erected up to the 15th floor, and the floor slab concrete was placed after the concrete was placed in the CFT columns. The concrete strengths were 24 N/mm^2 underground, 42 N/mm^2 for the column filling, and 21 N/mm^2 (lightweight concrete) above ground.

2.2. Field measurement

Field ambient response measurements were conducted at four different construction stages. Fig. 3 shows the transitions of the construction stages. Stages I and II measurements were conducted to compare the dynamic characteristics before and after concrete filling of the CFT columns up to the 11th floor. At this point, the floor slab concrete for each story had not yet been placed. Stage III was when the main structure of the building was completed. Concrete filling of CFT columns and slab concrete placing of each story were finished, and the dynamic characteristics of the main structure itself were checked. A tower crane was installed from Stage I to Stage III.

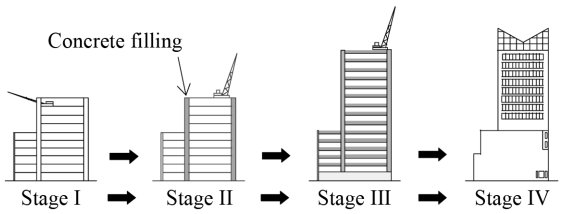


Figure 3. Transition of construction stage.

Stage IV was at completion of the building, and the influence of non-load-bearing walls was checked. Servo-type accelerometers were used for ambient response measurement. With high sensitivity and resolution (10^{-6} V/g), a sufficient response signal was obtained. The sampling rate was set at 20 Hz, with a Nyquist frequency of 10 Hz. The duration of each record was 1,800 seconds.

The time series of each channel had 36,000 points. Full ambient response measurements of the CFT building took less than 6 hours to finish within the same day. At Stages I, II and III, eight accelerometers were installed at the top of the CFT building, and six accelerometers were installed below ground level.

At Stage IV, fourteen accelerometers were used for one setup with two accelerometers at the 15th floor as references. It is reasonably assumed that the floor was subject to lateral rigid body motion. The measured vibration was translated into equivalent motions at the desired corners. Accelerometers excluding reference accelerometers were used as roving sensors for the 1st, 2nd, 3rd and 4th setups. Three accelerometers were typically placed in the southeast (x direction) and northeast corners (x and y directions) from the 7th floor to the 15th floor as well as on the roof. Six accelerometers were placed at the 2nd, 4th and 6th floors.

The ambient data recorded during the field measurement was processed in the frequency domain afterwards. Power spectral density was estimated using full measurement data with a frame of 1024 data points. 512 spectrum lines, with frequency resolution of 0.01953 Hz, were calculated. A Hanning window was applied as usual with 66.7% overlap to increase the average number.

2.3. Modal identification with Frequency Domain Decomposition

2.3.1. Modal frequency & mode shape identification

Instead of using PSD directly, as with the classical frequency domain technique, the PSD matrix is decomposed at each frequency line via Singular Value Decomposition (SVD). SVD has a powerful property of separating noisy data from disturbance caused by unmodeled dynamics and measurement noise. For the analysis, the Singular Value plot, as functions of frequencies, calculated from SVD can be used to determine modal frequencies and mode shapes. It has been proved[8] that the peaks of a singular value plot indicate the existence of structural modes.

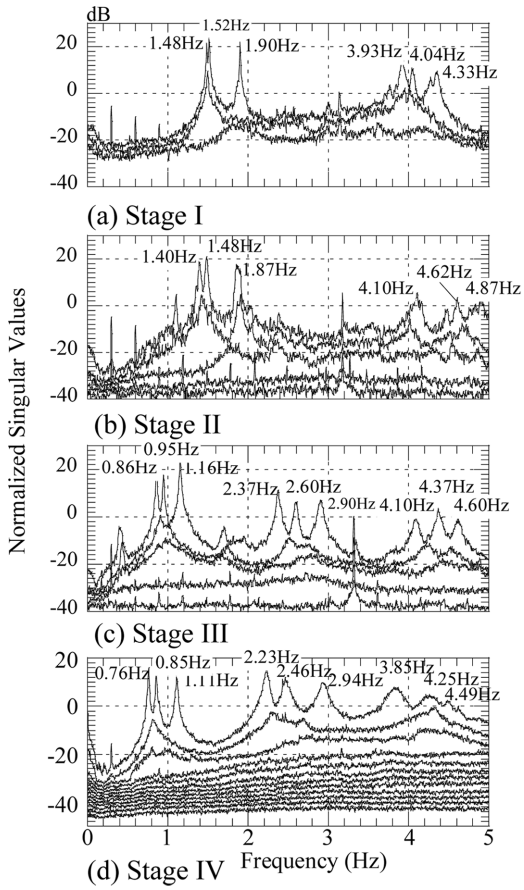


Figure 4. Singular value plot at the CFT building.

The singular vector corresponding to the local maximum singular value is unscaled mode shape. This is exactly true if the excitation process in the vicinity of the modal frequency is white noise. One of the major advantages of the FDD technique is that closely-spaced modes, even repeated modes, can be dealt with without any difficulty. The only approximation is that orthogonality of the mode shapes is assumed. Fig. 4 presents the SV Plots of the CFT building at different stages.

Table 1 gives nine identified modal frequencies. Fig. 5 depicts the corresponding nine mode shapes. In the FDD technique, the PSD matrix is formed first from ambient response measurements. ARTeMIS was used as the analysis software.

2.3.2. Modal damping estimation

One of the major objectives of the research project was to estimate the modal damping of the CFT building. The basic idea of the FDD method is as follows.[9] The singular value in the vicinity of natural frequency is equivalent to the power PSD function of the corresponding mode (as a SDOF system). This PSD function is identified around the peak by comparing the mode shape estimate with the singular vectors for the frequency lines around the peak. As long as a singular vector is found that has a high Modal

Table 1. Natural frequency of CFT building

Mode	Natural Frequency (Hz)			
	Stage II	Stage III	Stage IV	Stage V
1st	1.48	1.40	0.86	0.76
2nd	1.52	1.48	0.95	0.86
3rd	1.90	1.87	1.16	1.11
4th	3.93	4.10	2.37	2.23
5th	4.04	4.62	2.60	2.47
6th	4.33	4.87	2.90	2.94
7th	-	-	4.10	3.85
8th	-	-	4.37	4.26
9th	-	-	4.60	4.47

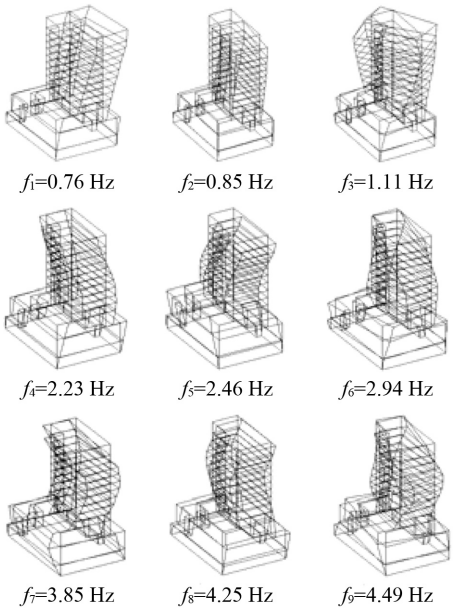


Figure 5. Mode shape of the CFT Building at Stage IV.

Amplitude Coherence (MAC) value with the mode shape, the corresponding singular value belongs to the SDOF function. If at a certain line none of the singular values has a singular vector with a MAC value larger than a certain limit value, the search for matching parts of the PSD function is terminated. Fig. 6 gives a typical "bell" of the SDOF system - the first and second modes of the CFT building. The remaining spectral points (the unidentified part of the PSD) are set to zero. From the fully or partially identified SDOF spectral density function, the natural frequency and the damping ratio can be estimated by taking the PSD function back to the time domain by inverse FFT as a correlation function of the SDOF system, as shown in Fig. 7. From the free decay function, the natural frequency and the damping are found by the logarithmic decrement technique. In the FDD, the power spectral density functions should be estimated via discrete Fourier transform (DFT) before the SVD. It is well known that leakage error in PSD estimation always takes place

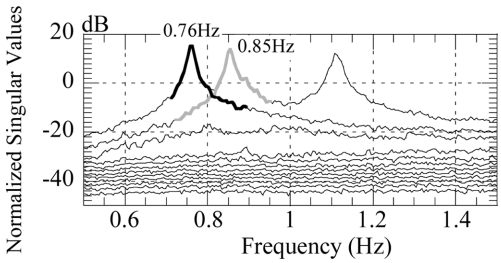


Figure 6. Singular value plot of the CFT building at Stage IV (Frequency ranges 0.5~1.5 Hz).

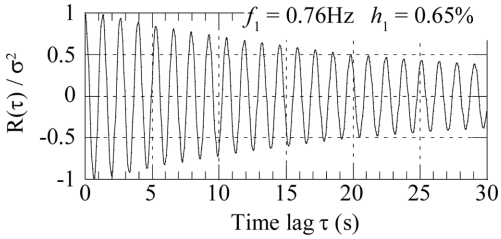


Figure 7. Correlation function of the 1st mode at Stage IV.

due to data truncation of DFT. Leakage is a kind of bias error, which cannot be eliminated by windowing, e.g., by applying a Hanning window, and is harmful to the damping estimation accuracy, which relies on the PSD measurements.

The bias error caused by leakage is proportional to the square of the frequency resolution.[10] Therefore, increasing frequency resolution is a very effective way to reduce leakage error. Thanks to the volume of data taken at field response measurements, we can afford to use more data, i.e., increase frequency resolution, in PSD computation. In order to show the influence of the frequency resolution on the damping estimation accuracy, 256, 512, 1024, 2048 and 4096 data points were used to calculate the PSD functions. The corresponding frequency resolutions were 0.0783, 0.0392, 0.0195, 0.00977 and 0.00488 Hz, respectively. Fig. 8 presents the changes of the damping ratios with the number of data points used for PSD calculation at Stage IV. It is very interesting to observe that, as predicted by the theory of random data procession, the damping ratios of all modes decrease, while the number of data points, or frequency resolution, increase. It appears that damping estimates converge when the number of data points is large enough (up to 4096 or 8192). Table 2 shows the damping ratios of all construction stages with enough data points to be used for PSD calculation.

2.4. Modal identification by FEM analysis and FE modal updating based on field measurement results

2.4.1. FEM model

The FEM models were based on the design documents. For the model before placing concrete in the CFT col-

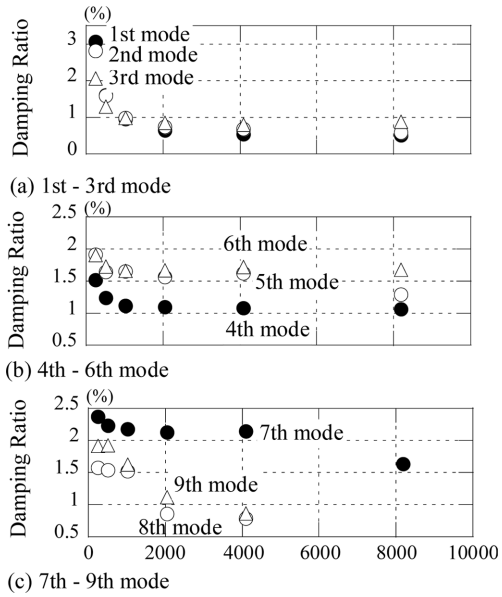


Figure 8. Changes of damping ratio vs. data points at Stage IV.

umns, as Stage I, the columns were of steel pipe and the CFT columns were of steel pipe portions, and the columns, which compounded the concrete, as Stage II. For the model up to the 11th floor (Stages I and II), two cases were compared: the pedestal assumed as pinned, and the pedestal assumed as fixed. After the 15th floor of the building was completed and the slab concrete was placed, as Stage III, the field measurement results were compared for the model with steel floor beams and that with composite beams. The assumption of a synthetic beam was taken as the form where 1/10 of the length of the beam was derived from Design Recommendations for Composite Constructions.[11] The underground portion was modeled as CFT columns and RC walls. The RC walls of the underground portion were modeled as shell elements. Moreover, the analysis model upon building completion, as Stage IV, considered two cases: the stiffness of the main structure only, and the stiffness of the main structure as well as the stiffness of the exterior walls. The non-load-bearing curtain walls were modeled as spring elements, and the stiffness was determined so that the first mode natural frequency from the field measurement agreed with the FEM value. The general-purpose structural analysis program SAP-2000 was used as the analysis software.

Table 2. Damping Ratio of CFT building

Mode	Damping Ratio (%)			
	Stage I	Stage II	Stage III	Stage IV
1st	0.27	0.75	0.53	0.65
2nd	0.32	0.70	0.65	0.74
3rd	0.18	0.80	0.59	0.84
4th	0.53	0.81	0.61	1.10
5th	0.40	0.60	0.72	1.56
6th	0.99	1.25	0.84	1.67
7th	-	-	0.86	2.12
8th	-	-	0.76	0.85
9th	-	-	0.79	1.11

2.4.2. FEM modal updating

The vibration modes obtained by FEM analysis at building completion (Stage IV) are shown in Table. 3. In the FEM analysis, the building's stiffness was estimated only for the members of the main structure. As a result, the FEM results are evaluated slightly smaller than the actual values. The stiffness of the building's exterior walls was therefore added so that the first vibration mode was nearly identical to the actual value. As a result, satisfactory agreement was obtained up to the sixth vibration mode. The stiffness of the walls at this stage was 9.8 kN/cm/m. This is reported in a paper that describes a survey investigation on the stiffness of ALC outer walls.[12] The stiffness used for this analysis is almost the same as in this paper.

The lowest natural frequency for Stage IV (at building completion) was measured as 0.76 Hz, where *Y*-dir. translational motion is predominant. Survey investigations of the natural period of multi-story buildings in Japan[13] show that the lowest natural frequency f_1 (Hz) of a building with a height H (m) is approximated by the following expression.

$$\begin{cases} f_1 = \dfrac{H}{0.020} (\text{Steel structures})^8 \\ f_1 = \dfrac{H}{0.015} (\text{Steel encased reinforced concrete structures})^8 \end{cases}$$

Table 3. Nine mode shapes and their natural frequencies of a CFT Building obtained by FEM analysis and FDD (Stage IV)

Mode									
Frequency (Hz)	f_1	f_2	f_3	f_4	f_5	f_6	f_7	f_8	f_9
FEM	0.74	0.82	1.02	1.92	2.18	2.45	-	-	-
Tuned FEM	0.76	0.87	1.15	2.14	2.53	3.02	3.85	4.26	4.67
FDD	0.76	0.86	1.11	2.23	2.47	2.94	3.85	4.26	4.47

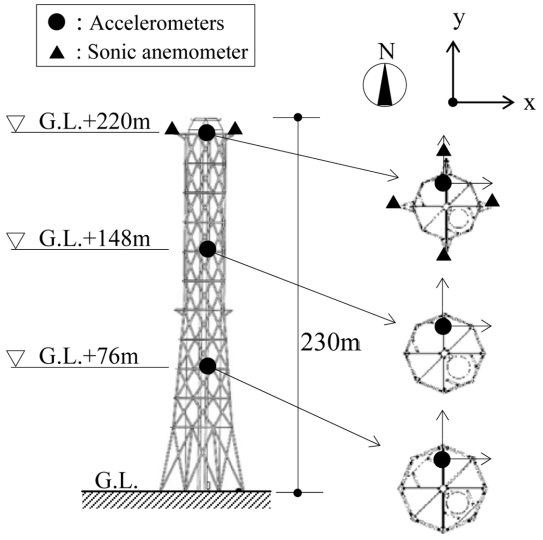


Figure 9. Elevation of chimney.

The height of this building is 59.15 m. Thus, the frequency derived from this formula for steel structures is 0.85 Hz, and that for steel encased reinforced structures is 1.13 Hz. These results show that the natural frequencies of this building are close to those for steel structures.

3. Efficiency of Tuned Mass Damper by Checking Dynamic Characteristics of a Chimney[14,15]

3.1. Field measurement set-up

Ambient response measurements of a 230 m-high chimney were conducted to investigate its dynamic characteristics. Fig. 9 shows the elevation and plan of the tested chimney, consisting of steel trusses and a concrete funnel. The chimney has an octagonal cross section.

Accelerometers were installed on three different levels, as shown in Fig. 9. Two horizontal components (x, y) and one vertical component (z) were measured at each level. A sonic anemometer was also installed at the top of the chimney. The sampling rate of the acceleration records was set at 100 Hz, and the ambient responses were measured for 90 minutes in total.

3.2. Modal identification by 2DOF-RD technique and FDD for ambient vibration

3.2.1. Dynamic characteristics of chimney estimated by 2DOF-RD technique

Fig. 10 shows the power spectrum density functions of accelerations at three different heights. Peaks corresponding to several natural frequencies are clearly shown.

At first, the general Random Decrement (RD) technique assuming a SDOF system was applied for modal identification using the ambient y-dir. acceleration records at the top level, GL+220 m. By processing with a numerical band-pass filter with a frequency range of 0.06~1.0 Hz,

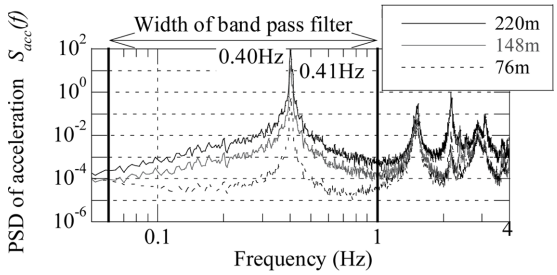


Figure 10. Power spectrum of tip acceleration (Y-dir).

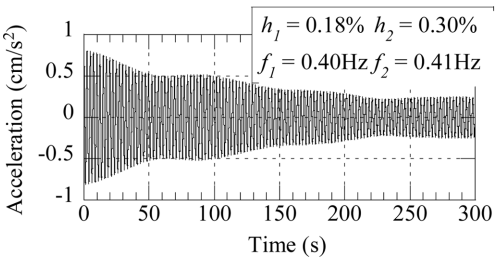


Figure 11. RD signature of tip acceleration (*Y*-dir.).

only the frequency components around the lowest peak near 0.40 Hz depicted in Fig. 10 were extracted. The initial amplitude of the acceleration to get the Random Decrement signature (RD-signature) was set at the standard deviation, s_{acc}. Fig. 11 shows the obtained RD-signature, where a beating phenomenon is clearly observed, suggesting two closely located predominant frequency components. By carefully studying the peak near 0.4 Hz, it is seen that there are actually two peaks: at 0.40 Hz and 0.41 Hz. These peaks are named f_1 and f_2, respectively, in this paper. The general RD technique assuming a SDOF system can efficiently evaluate the damping ratio and the natural frequency only for a well-separated vibration mode, but not for the above case. In order to evaluate the two closely located two vibration modes, the 2DOF-RD technique is proposed, where the superimposition of the two SDOF systems with different dynamic characteristics is made. The RD signature shown in Fig. 11 was approximated by superimposition of the two different damped free oscillations as follows:

$$R_i(t) = \frac{x_{0_i}}{\sqrt{1-h^2}} e^{-h_i \omega_i t} \cos(\sqrt{1-h^2}\,\omega_i t - \phi_i)$$

$$R(t) = \sum_{i=1}^{2} R_i(t) + m$$

where $R(t)$: RD signature, $R_i(t)$: i-th mode component (i = 1 and 2), x_{0_i} : initial value of i-th mode component, h_i: i-th mode damping ratio, ω_i: i-th mode circular frequency, t: time, ϕ_i: phase shift, and m: mean value correction of RD signature.

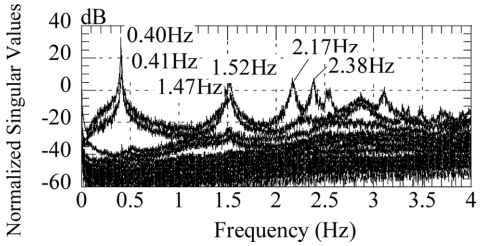


Figure 12. Frequency distribution of singular value.

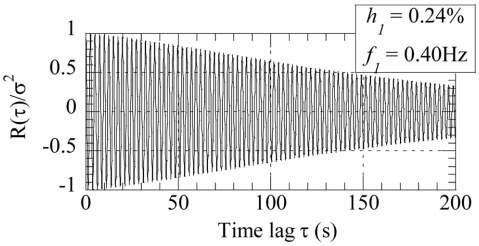


Figure 14. Correlation function obtained by FDD.

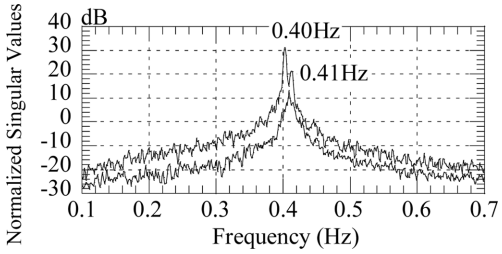


Figure 13. Frequency distribution of singular value (Close-up: frequency range 0.1~0.7 Hz).

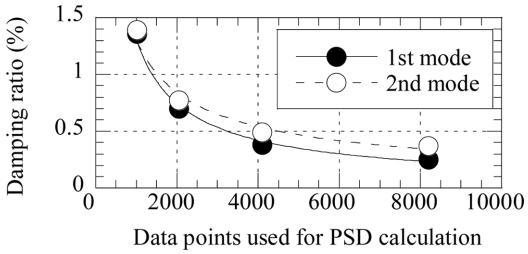


Figure 15. Variations of damping ratio with PSD data points.

The approximation was made by the least-square method, and the damping ratio and the natural frequency of the chimney were estimated at 0.18% and 0.40 Hz for the 1st mode, and 0.30% and 0.41 Hz for the 2nd mode. The dynamic characteristics of the 3rd and 4th modes were also estimated by the 2DOF-RD technique.

3.2.2. Dynamic characteristics of chimney estimated by FDD

The FDD method was applied to the six horizontal components of the acceleration responses at the three different heights to evaluate the chimney's dynamic characteristics. Fig. 12 shows the frequency distribution of the singular value obtained by the FDD method. Fig. 13 is a close-up in the range of 0.1~0.7 Hz, where the upper line shows two peaks at 0.40 Hz and 0.41 Hz, corresponding to f_1 and f_2 in 3.2.1. The lower line has a peak between 0.40 Hz and 0.41 Hz, and the right-side slope can be connected to the first peak of the upper line, and the left to the second peak. This forms a "bell" as already shown in Fig. 6, so the combination of the upper and lower lines can closely identify the located modes.

Fig. 14 shows the auto-correlation function of the 1st mode obtained by the inverse FFT for the separated peak as above. Fig. 15 shows the variations of the damping ratios of the lowest two modes with the number of data points used for PSD calculation. The damping ratios converge to precise values with increase in the number of data points.

Table 4 shows the dynamic characteristics of the chimney obtained by the FDD method with enough PSD data points and by the RD technique, where the 2DOF-RD technique was used for the 1st, 2nd, 3rd and 4th modes. These results show fairly good agreement between the FDD and 2DOF-RD techniques, except for the 3rd-mode damping ratio.

Table 4. Dynamic characteristics of chimney

Mode	Natural Frequency (Hz)		Damping Ratio (%)	
	RD	FDD	RD	FDD
1st	0.40	0.40	0.18	0.24
2nd	0.41	0.41	0.30	0.39
3rd	1.47	1.47	0.83	0.3
4th	1.53	1.52	0.85	0.91
5th	2.17	2.17	0.55	0.65
6th	2.38	2.38	0.42	0.39
7th	-	2.87	-	-
8th	-	3.10	-	0.77

3.3. Modal identification for wind-induced vibration

Wind-induced response measurements were also performed to identify the dynamic characteristics during strong wind. Based on the above results of ambient response measurements, a TMD was installed in the top of the steel tower. In this paper, the variation of dynamic characteristics before/after installing the TMD is investigated.

Fig. 16 shows the trajectory of acceleration during strong wind. The mean wind speed is 20.8 m/s for the acceleration without TMD and 20.7 m/s for the acceleration with TMD, and both wind directions were NNE. The acceleration in the across-wind direction before installing the TMD is about 40 cm/s^2 and is larger than that in the along-

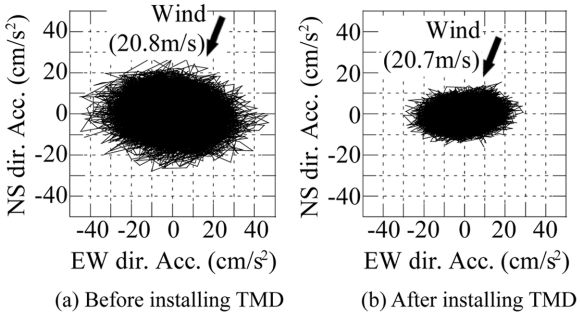


Figure 16. The trajectory of acceleration during strong wind.

wind direction (about 25 cm/s^2). When comparing the accelerations in the across-wind direction before/after installing the TMD, the maximum acceleration after installing the TMD is smaller than that before installing the TMD. This is considered to be the effect of the TMD.

Field measurement in strong wind was performed when the wind direction was almost S or N. The relationships between the standard deviation of tip acceleration and the mean wind speed are shown in Fig. 17. Although the standard deviation of tip acceleration in the along-wind direction fluctuates when the mean wind speed is low, the tip acceleration after installing the TMD is about 35% smaller than that before installing the TMD as shown in Fig. 17(a). In the across-wind direction, it seems that the TMD had no effect, as shown in Fig. 17(b).

Fig. 18 shows the variation of the damping ratio of along and across-wind direction with the mean wind speed estimated by the RD technique. In both along- and across-wind directions, the damping ratio before installing the TMD clearly increases with increasing wind speed. The damping ratios after installing the TMD increase as compared with that before installing the TMD in both directions. And the damping ratio for the across-wind direction is larger than that for the along-wind direction.

The length of the acceleration record used for FDD is about 4 hours, and combined 20 samples (the length of 1 sample is about 700 seconds). Fig. 19 shows the singular value distribution obtained by FDD for the acceleration records before/after installing the TMD during strong wind. The number of data points used for PSD calculation is 16,384 (df = 0.006 Hz) in both cases. The two closeest peaks exist in the singular value distribution as 1st mode peak and 2nd mode peak. The natural frequency estimated from the singular value distribution after installing the TMD moved to a lower frequency than that before installing the TMD.

Fig. 20 shows the variations of damping ratio (1st and 2nd mode) with the number of data points used for PSD calculation during strong wind. With increasing numbers of data points used for PSD calculation, the damping ratios decrease and converge to constant values.

The damping ratios before installing the TMD for along- and across-wind direction converged to about 0.4% and 0.6%, and that after installing TMD converged to about 1.2% and 1.1%, respectively. As shown in these figures, the efficiency the TMD was clearly identified at damping ratios of the 1st and 2nd modes. Fig. 21 shows the

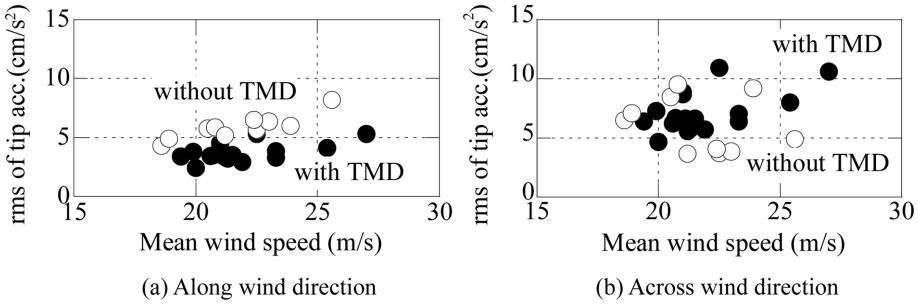


Figure 17. The relationships between standard deviation of tip acceleration and mean wind speed.

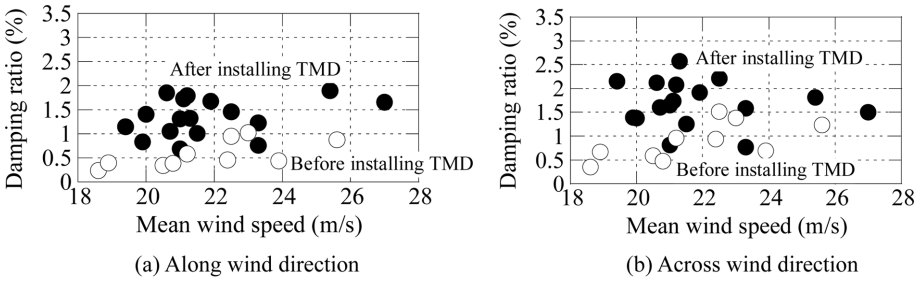
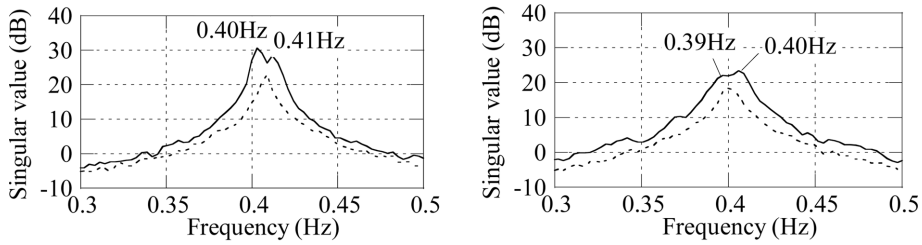
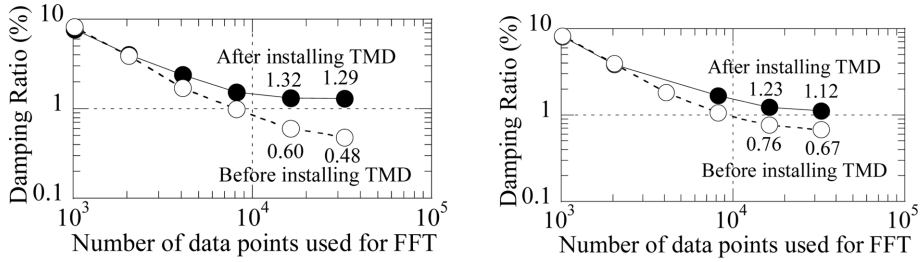


Figure 18. The variation of the damping ratio estimated by RD technique with the mean wind speed.



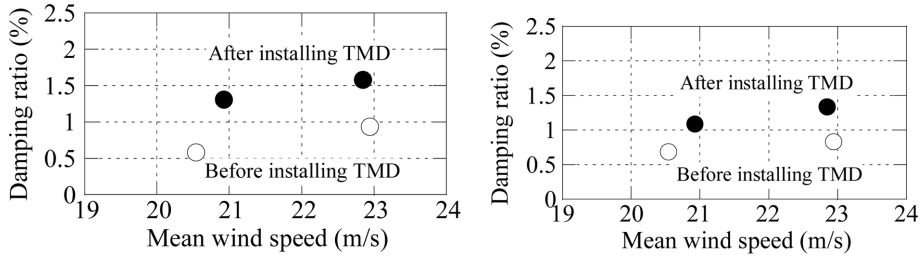
(a) Before installing TMD (b) After installing TMD

Figure 19. Singular values obtained by SVD of cross-spectrum density function.



(a) 1st mode (b) 2nd mode

Figure 20. The variations of damping ratio with PSD data points (During strong wind).



(a) Along wind direction (b) Across wind direction

Figure 21. The variations of damping ratio with mean wind speed.

variation of the damping ratio, which is identified with 16,384 data points used for PSD calculation, with the mean wind speed. With increasing mean wind speed, the damping ratio also increased, although the change of the mean wind speed is small.

Damping ratios identifying two different methods are shown in Fig. 22. The mean wind speeds were 21.7 m/s for before installing the TMD and 21.8 m/s for after installing the TMD, and the same acceleration record was used for RD technique and FDD. The results obtained from the RD technique were the mean value of the damping ratios of all samples for along-wind direction shown in Fig. 18(a). The damping ratios obtained from FDD were the mean value of two samples for along-wind direction shown in Fig. 21(a). From RD technique, the damping ratio increased from 0.57% to 1.34%, and from FDD, the

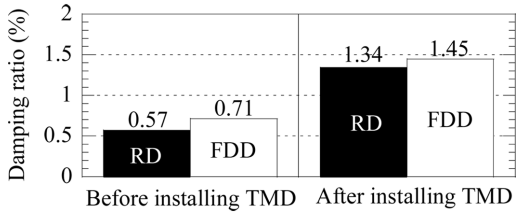


Figure 22. The damping ratios identified two different methods.

damping ratio increased from 0.71% to 1.45. As shown in the previous section, the damping ratio for ambient vibration is about 0.2% and is smaller than that during strong wind. This difference results from the difference between the acceleration amplitudes for ambient response and

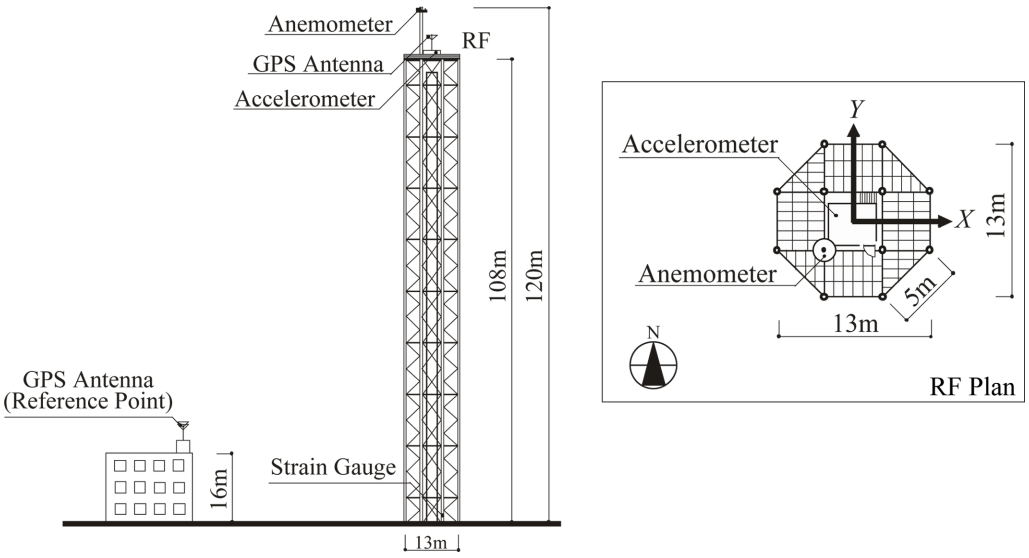


Figure 23. A 108 m high steel tower for full-scale measurements.

wind-induced response.

4. Wind-induced Response Measurement using RTK-GPS and Integrity Monitoring

4.1. Outline of field measurements

Field measurements were performed on a high-rise steel tower belonging to the Urban Development Corporation. As shown in Fig. 23, an anemometer, an RTK-GPS antenna and accelerometers were set on top of a 108 m-high steel tower, and another RTK-GPS antenna was set as the reference point on top of a rigid 16 m-high RC building next to the tower. In addition, to measure member stresses, strain gauges were set in the base of the tower. Before measurement, the zero-position was carefully defined as the mean value of almost three months of data. These data satisfied the following condition to minimize the wind and solar heating effects: PDOP less than 1.5, mean wind speed less than 1m/s and data from 0:00~5:00 am.

4.2. Wind-induced responses during Typhoon 0221

Fig. 24 shows the temporal variations of wind and response data every 10 min during Typhoon 0221. The wind direction was mostly NNW-NW when the typhoon came closest, and the wind speed reached its maximum, as shown in Fig. 24(a). The maximum wind speed was about 22 m/s and the peak gust wind speed was about 30 m/s, as shown in Fig. 24(b). The acceleration data shown in Fig. 24(c) varies following the variation of wind speed shown in Fig. 24(b), and the RTK-GPS displacement shown in Fig. 24(d) also follow the variation of acceleration data. Here, only the RTK-GPS data obtained under the conditions of PDOP less than 3 were analyzed. Fig. 25 shows an example of the temporal variation of the tower's

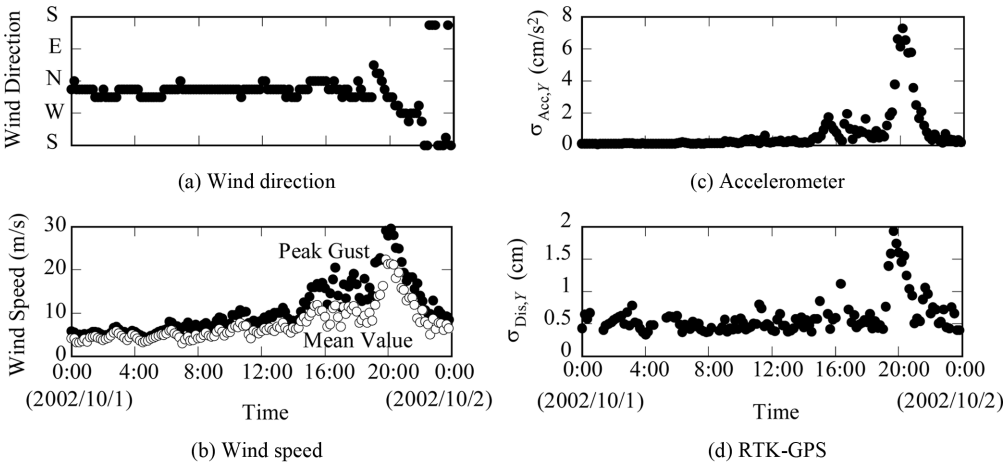


Figure 24. Temporal variations of 10 min mean values of wind speed and response of the tower.

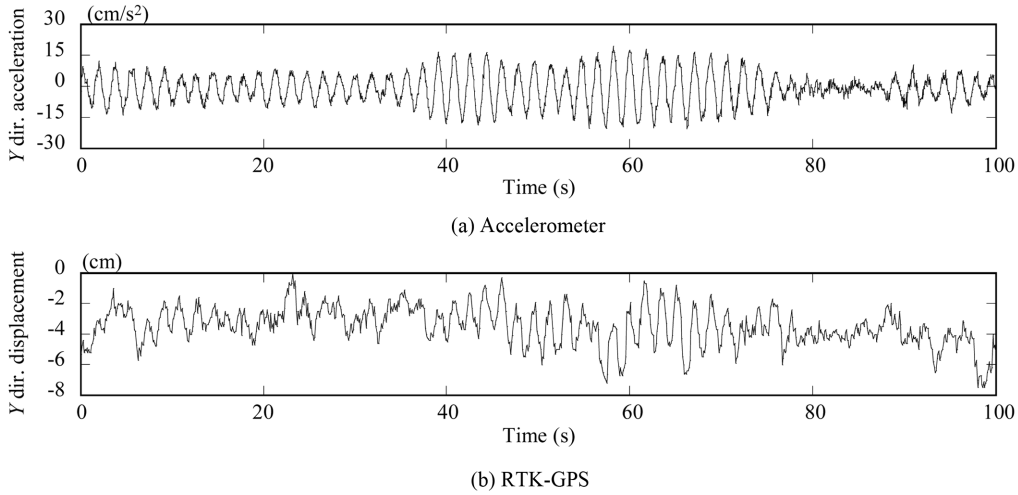


Figure 25. Examples of temporal variations of wind-induced responses of the tower during Typhoon 0221.

response in the *Y*-direction, which coincides with wind direction NW when the typhoon was located closest to the site. The RTK-GPS data is the sum of the static displacements of about 4 cm, the fluctuating component with a long period, i.e., about 20 seconds, and that with a dominant frequency equal to the lowest natural frequency of 0.57 Hz. The acceleration record seems to correspond closely to the predominant frequency component of the displacement by RTK-GPS.

Fig. 26 shows an example of the tip displacement and acceleration locus showing static component and fluctuating component. The RTK-GPS could measure not only dynamic components but also static components of about 5 cm corresponding to wind direction.

Fig. 27 shows the power spectrum densities of the tip responses. The power spectral density of the acceleration was converted to that of displacement multiplied by $(2\pi f)^{-4}$ for comparison with the displacement by the RTK-GPS. For *X* direction response as shown in Fig. 27(a), there are two peaks, and the accelerometer and RTK-GPS results show the same tendency. Both spectra in Fig. 27(b) have a peak at 0.57 Hz corresponding to the lowest natural frequency of the tower.

However, those of the displacement by the RTK-GPS show almost constant energy in the higher frequency range, which is attributed to the background noise of the RTK-GPS in both figures.

The vibration characteristics are estimated by the RD technique. Figs. 28(a) and (b) show the random decrement signature obtained by this technique from the acceleration record and the RTK-GPS displacement record in the *Y* direction, respectively. The damping ratio and the natural frequency were estimated using the least square fitting to a SDOF system. The lowest natural frequency was estimated at 0.57 Hz for both cases. The damping ratio was estimated at 0.62% for the acceleration record and 0.70% for the RTK-GPS displacement.

Since the RTK-GPS can measure the static displacement, the deformation of the tower caused by the solar heating effect could also be detected. Fig. 29 shows the tower deformation caused by solar heating on a calm and clear day. Each plot indicates the preceding hour's mean

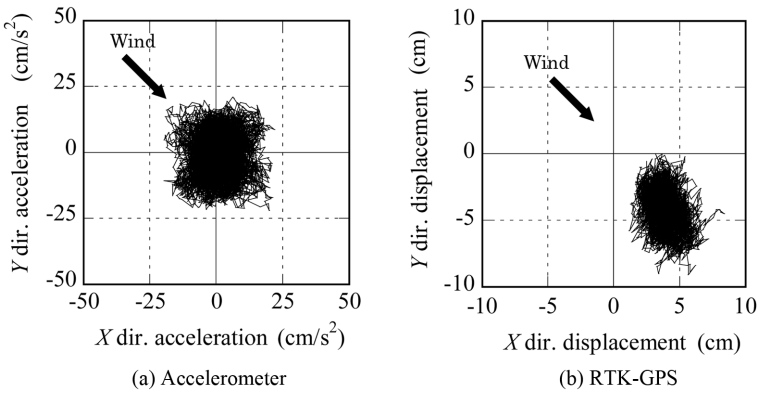


Figure 26. Example of tip locus during Typhoon 0221.

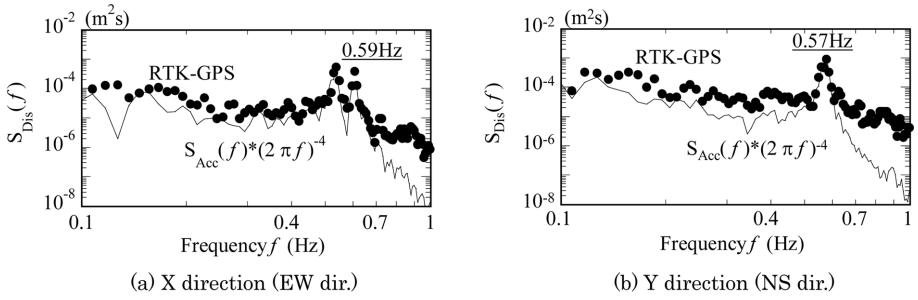


Figure 27. Power spectra of tip displacement during Typhoon 0221.

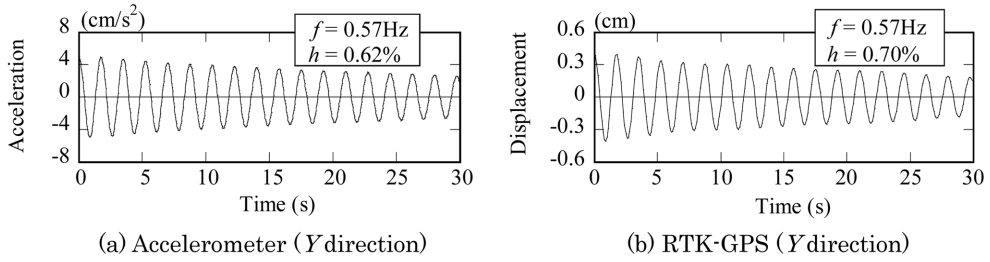


Figure 28. Random decrement signature obtained by RD technique.

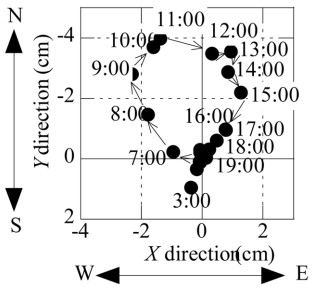


Figure 29. Tower deformation caused by solar heating effect.

displacement with time. Just after sunrise, the tower began to move about 4 cm in the NW direction. The top of the tower moved in an almost circular shape in the daytime, and returned to its zero point after sunset.

4.3. FEM analysis of tower

An FEM tower model based on the design documents was created in the computer. SAP2000 was used for the FEM analysis. The total mass of the upper structure was 7.3×10^5 kg. The 1st mode natural frequency of the FEM model was calculated to be 0.57 Hz: exactly the same as the full-scale result. The lowest three modes of the FEM model for the X direction are shown in Fig. 30. In addi-

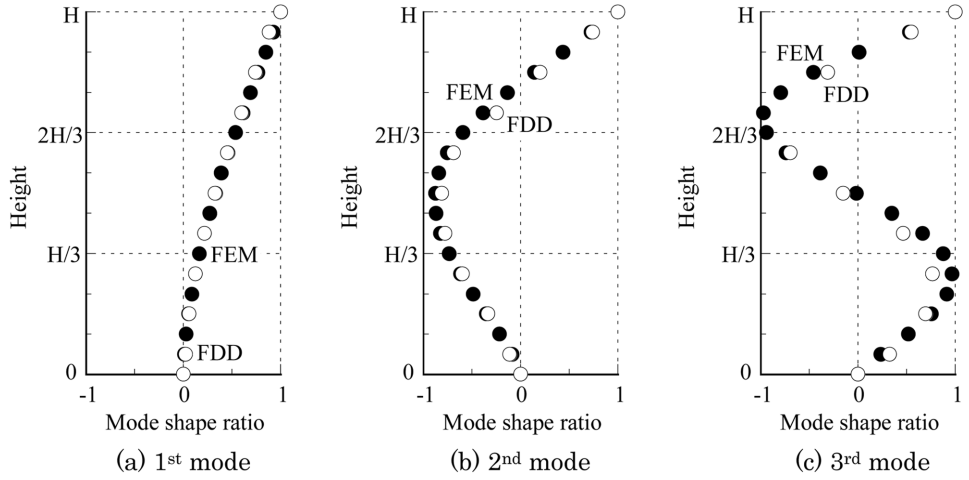


Figure 30. Mode shapes obtained by FEM and FDD.

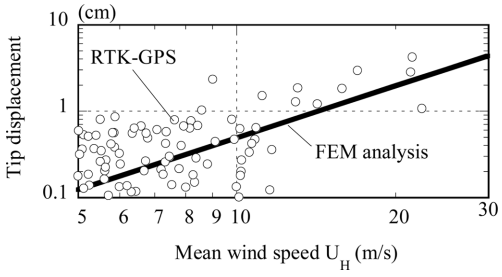


Figure 31. Changes of mean tip displacement by mean wind speed.

tion, ambient vibration tests were performed to investigate the vibration characteristics of the tower using the FDD (Frequency Domain Decomposition) method.[16,17] The lowest three modes obtained by FDD are also shown in Fig. 30. These results show good agreement.

Fig. 31 indicates the relation of the mean displacements obtained by GPS and FEM analysis. In the FEM analysis, mean wind force F_z at height z was evaluated from $F_z = rU_z^2CA/2$, where the mean wind speed U_z was estimated assuming a power-law index $a = 0.2$, and the wind force coefficient C was estimated from the following equation.[18]

$$C = 4.0\phi^2 - 5.9\phi + 4.0 \tag{1}$$

Here, r is air density, A is projected area, and f is solidity ratio (in this case, $f = 0.65$). Fig. 31 shows good agreement between the FEM analytical result and the GPS full-scale results, although the full-scale results are somewhat scattered. The GPS displacement used for the analysis satisfied the following conditions: most frequent wind direction is N and the weather is cloudy or rainy due to a minimized solar heating effect.

4.4. Hybrid use of FEM analysis and RTK-GPS for integrity monitoring

The above results encourage us to evaluate the member stresses by hybrid use of FEM analysis and RTK-GPS to create a real time monitoring system to establish the tower's integrity. The tip displacement obtained by GPS can be easily converted into member stresses based on the FEM analysis as shown in Eq. (2) and Fig. 32.

$$\sigma = \sigma_{x_{DIS}=1} \times x_{GPS} + \sigma_{y_{DIS}=1} \times y_{GPS} \tag{2}$$

where s is member stress by hybrid use of FEM analysis and GPS (only for axial forces), $s_{x(y)DIS=1}$ is member stress calculated by FEM analysis when tip displacement is 1 cm for $x(y)$ direction, $x(y)_{GPS}$ is tip displacement measured by RTK-GPS.

The system can monitor the stresses in all members during typhoons, and can even send out a warning if one of the member stresses exceeds an allowable level. For example, the stresses in members at the tower base shown in Fig. 33 were calculated from the temporal variation of the GPS tip displacement. Fig. 34 shows the temporal variations of stresses measured by strain gauges and virtually monitored by hybrid use of the FEM and RTK-GPS.

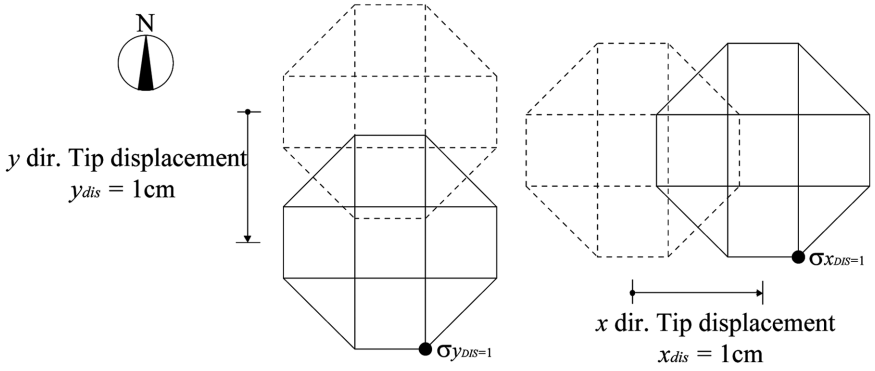


Figure 32. Solution of member stresses by hybrid use of FEM analysis and GPS (for "Outer column").

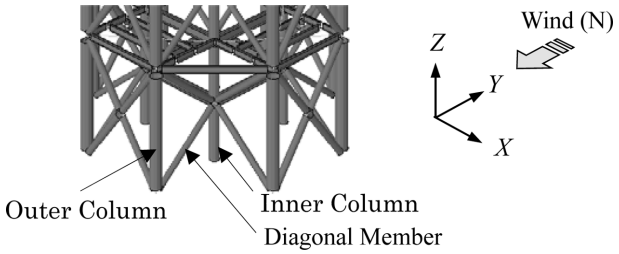


Figure 33. Members detected by hybrid use of FEM analysis and RTK-GPS.

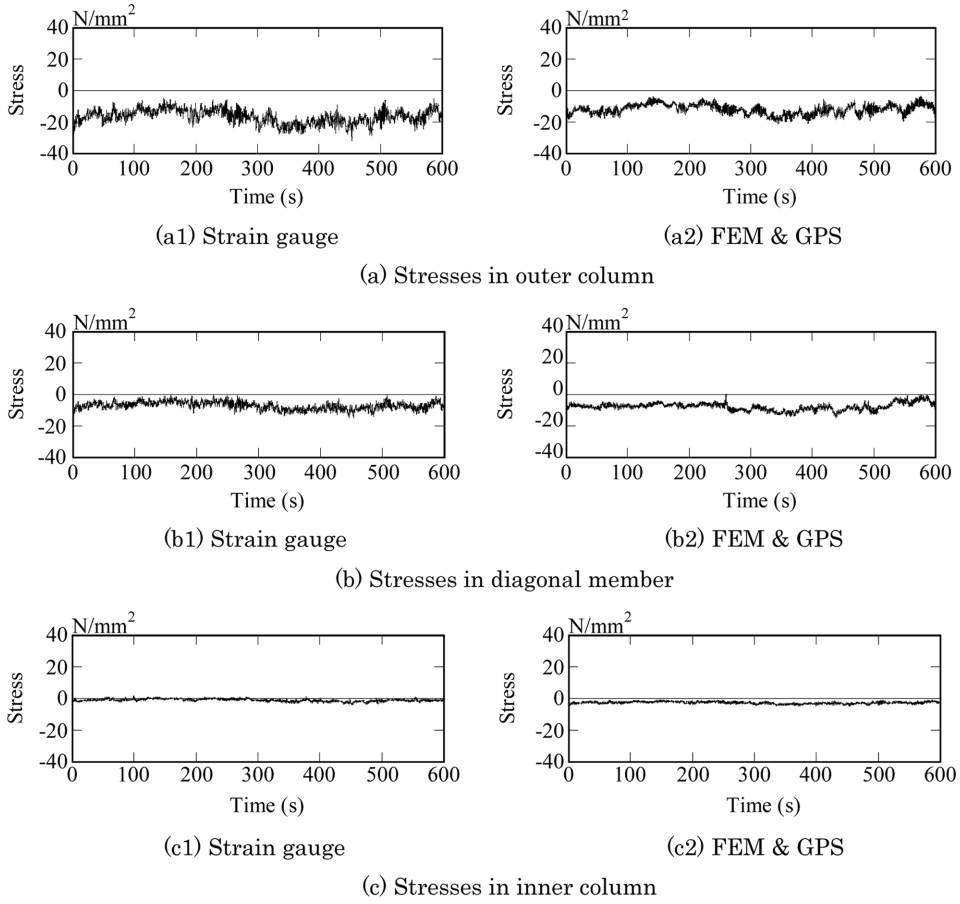


Figure 34. Temporal variations of stresses by field measurement and hybrid use of FEM analysis and RTK-GPS.

The results shown in Fig. 34 are member stresses converted from GPS displacement during Typhoon 0221. They don't include the stresses caused by tower dead load. These members, i.e., inner column, outer column and diagonal member shown in Fig. 33, were compressive members as shown in Fig. 34. Reflecting the fluctuation of wind forces, the outer column stresses (Fig. 34(a)) and diagonal member stresses (Fig. 34(b)) fluctuated. However, the inner column stresses (Fig. 34(c)) fluctuated much less than the outer column and diagonal member stresses, and it bore mainly vertical load. They show good agreement with member stresses obtained from strain gauges and hybrid use of FEM analysis and GPS.

Fig. 35 shows the power spectrum of member stresses obtained by strain gauges and hybrid use of FEM analysis and GPS. For the power spectrum of stresses in the outer

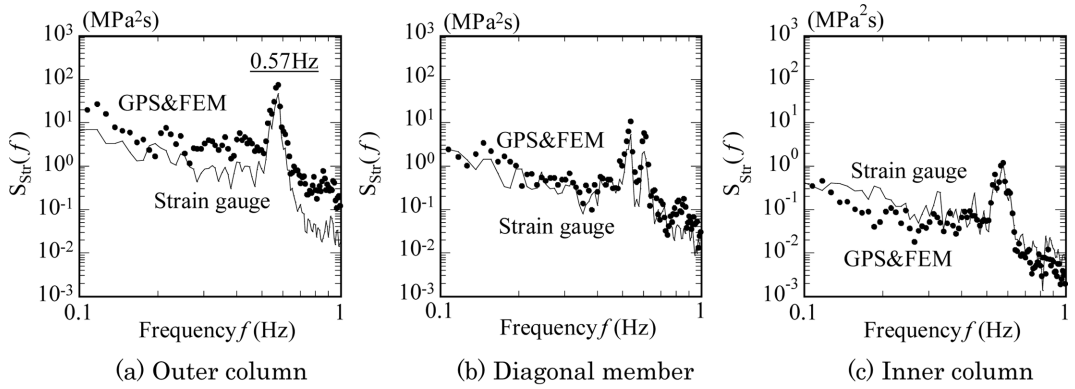


Figure 35. Power spectrum of member stresses during Typhoon 0221.

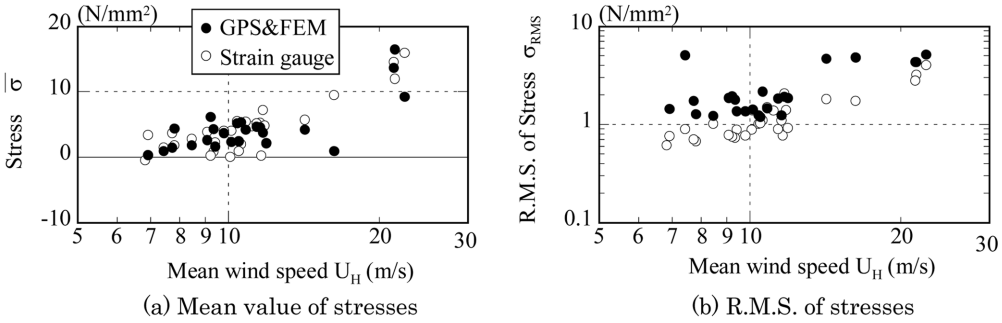


Figure 36. Changes of stresses of outer column by mean wind speed.

column as shown in Fig. 35(a), that by hybrid use of FEM analysis and GPS showed higher energy in all parts than that by strain gauge. However, for the power spectrums of stresses in the diagonal member (Fig. 35(b)) and in the inner column (Fig. 35(c)), that by strain gauge and that by hybrid use of FEM analysis and GPS showed good agreement.

Fig. 36 shows changes of stresses in the outer column with changes in mean wind speed. As shown, changes in mean stresses become large when mean wind speed becomes large. The results of strain gauge and hybrid use of FEM analysis and GPS show fairly good agreement. When mean wind speed is less than about 10 m/s, R.M.S values of stresses in the outer column by hybrid use of FEM analysis and GPS are almost constant and are higher than those by strain gauge. This is considered to be due to the background noise of RTK-GPS.[3-5]

5. Amplitude Dependency of Dynamic Characteristics for High-rise Building

Continuous Field measurements of a high-rise steel building have been conducted to investigate the characteristics of both wind-induced response and seismic response. Fig. 37 shows an elevation and a plan of the measured building, which is in the Shinjuku area of Tokyo. It is 133.5 m high and its aspect ratio is around 4. Accelerometers are installed on its top floor, and their sampling ratios are set at 20 Hz. In addition, to measure the static displacement, especially for wind-induced response, a GPS antenna is installed at the top of the building, and its sampling ratio is also set as 20 Hz. Fig. 38 shows the power spectrum density function of tip displacement in the EW direction measured by the GPS system. The figure compares the P.S.D in a moderate wind with the P.S.D in a strong wind. The mean wind speed at the top of a neighboring building located about 230 m from this building was about 25 m/s. A peak corresponding to the 1st natural frequency at 0.38 Hz can be clearly seen. Fig. 39 shows a time history of tip displacement measured by the GPS system during the 2011 Tohoku Earthquake off the Pacific coast. The maximum tip displacements for the NS and

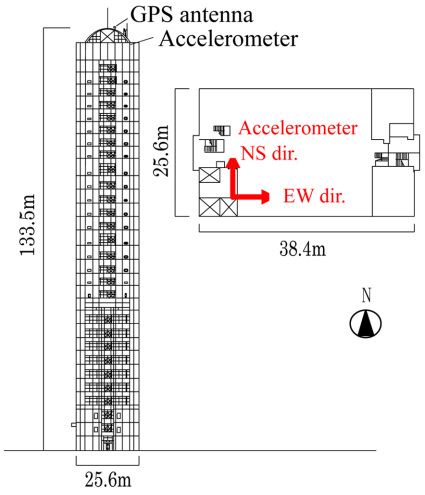


Figure 37. Elevation and plan of high-rise building.

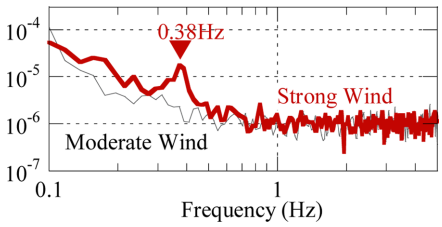


Figure 38. P.S.Ds of displacement by GPS for wind-induced response (EW direction).

EW directions were 35.5 cm and 28.6 cm, respectively. Fig. 40 shows the amplitude dependency of the natural frequencies of the building for the wind-induced response and seismic response measured by the accelerometers and the GPS system. The RD technique was used for the natural frequency estimation for an ambient vibration record and an acceleration record during strong wind obtained by accelerometers. It can be seen that the natural frequencies for the EW and NS directions decreased with increasing amplitude. In the ambient and the strong wind conditions, i.e., the acceleration range (standard deviation

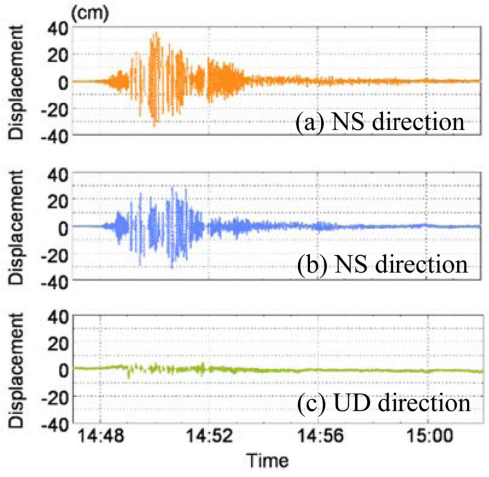


Figure 39. Time history of GPS displacement for the 2011 off the Pacific coast of Tohoku Earthquake.

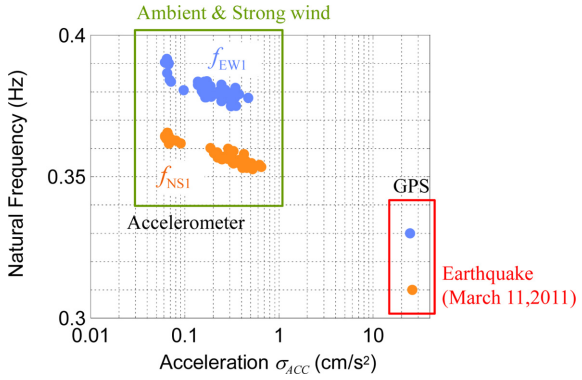


Figure 40. Amplitude dependency of natural frequency of high-rise building.

of acc.) of about 0.06~0.7 cm/s^2, the natural frequencies decreased from 0.39 to 0.37 for the EW direction and from 037 to 0.35 for the NS direction. For the earthquake record, the dominant frequencies of P.S.D of tip displacement measured by the GPS system were considered as the 1st mode natural frequencies of this building. The accelerations for the NS and EW directions were the standard deviations of acc. during the earthquake, and were calculated from the tip displacement measured by the GPS system. The natural frequencies of the seismic response were about 10% lower than those of the ambient and wind-induced responses.

6. Concluding Remarks

This paper has introduced the several examples of field measurement results that can be used for structural health monitoring. In the first project, field measurement results of 15-stories were shown. The simple FEM modal updating method based on the dynamic characteristics identified from the field measurement was introduced. The dynamic characteristics of a high-rise chimney were estimated by the FDD and 2DOF RD techniques using their ambient responses as the next project. The results were all satisfactory and agreed well. The damping ratios obtained by RD technique and FDD increase from 0.57% to 1.34% and from 0.71% to 1.45% after installing the TMD, respectively. The damping ratio for ambient vibration is about 0.2% and is smaller than that during strong wind. This difference results from the difference in amplitude of the acceleration between ambient response and wind-induced response. As the next example, the RTK-GPS system was used to measure not only the dynamic components but also the static component and quasi-static components of the wind-induced responses of a high-rise steel tower. Using FEM results and displacement by GPS, member stresses could be monitored in real time for integrity monitoring. As the last example, amplitude dependency of the dynamic characteristics for high-rise steel building were shown. Based on the results for the 2011 off the Pacific coast of Tohoku Earthquake, the natural frequencies of the seismic response were about 10% lower than those of the ambient and the wind-induced response.

Acknowledgement

We express our warm thanks to Prof. Yoshiaki Hisada (Kogakuin University), Dr. Shin-ichi Nakata (Asahi-kasei Homes Co., LTD.), Mr. Shun-ichi Naito (TAKU structural design company), Mr Takayoshi Ito (Tokyo Electric Power Services CO., LTD.), Mr. Kenji Masuda (Tokyo Electric Power Company) for their great support for the field measurements and for their valuable comments.

References

M. Çelebi, GPS and/or strong and weak motion structural response measurements - Case studies, Structural Engineering World Congress ‘98, San Francisco, Conference Proceedings on CD-ROM, 1998, T193-1, pp. 8.

Y. Tamura, M. Matsui, M. Uchiyama, K. Hibi and K. Ishihara, Feasibility study on observation of wind induced building responses by real-time-kinematic GPS - to construct comprehensive urban disaster prevention system, Summaries of Technical Papers of Annual Meeting, Architectural Institute of Japan, 1999, B-1, 203-204. (in Japanese).

Y. Tamura, A proposal of simultaneous monitoring of responses of tall buildings in an urban area during strong winds and earthquakes using GPS - Construction of a new disaster prevention system, Research in Architecture, 2000, 1-7. (in Japanese).

Y. Tamura, M. Matsui, L.C. Pagnini, R. Ishibashi and A. Yoshida, Measurement of wind-induced response of buildings using RTK-GPS. *Journal of Wind Engineering and Industrial Aerodynamics*, 90(2002), pp. 1783~1793.

Y. Tamura, A. Yoshida, R. Ishibashi, M. Matsui and L. C.

Pagnini, Measurement of wind-induced response of building using RTK-GPS and integrity monitoring, Proc. 2nd Int. Symposium on Advances in Wind & Structures, 2002, pp. 599~606.

Tamura, Y., Zhang, L., Yoshida, A., Cho, K., Nakata, S., and Naito, S., Ambient vibration testing & modal identification of an office building with CFT columns, 20th International Modal Analysis Conference, pp. 141~146, 2002.

Miwa, M., Nakata, S., Tamura, Y., Fukushima, Y., and Otsuki, T., Modal identification by FEM analysis of a building with CFT columns, 20th International Modal Analysis Conference, 2002.

Ibrahim, S. R. and Mikulcik, E. C., A Method for the Direct Identification of Vibration Parameters from the Free Response, Shock and Vibration Bulletin, pp. 183~198, No. 47, Pt. 4, Sept. 1977.

Brincker, R., Ventura, C. E. and P. Andersen, Damping Estimation by Frequency Domain Decomposition, Proc. of the 19th IMAC, 698-703, Feb. 2001.

Bendat, J. and Piersol, A., Random Data, Analysis and Measurement Procedures, John 'Wiley & Son, New York, USA, 1986.

Architectural Institute of Japan, Design Recommendations for Composite Constructions, 1985. (in Japanese).

Fukuwa, N., Nishizaka, R., Yagi, S., Tanaka, K, and Tamura, Y., Field measurement of damping and natural frequency of an actual steel-framed building over a wide range of amplitude. *Journal of Wind Engineering and Industrial Aerodynamics*, Vol. 59, pp. 325~347, 1996.

Architectural Institute of Japan, Damping of Structures, 2000. (in Japanese).

Masuda, K., Sasajima, K., Yoshida, A. and Tamura, Y., Dynamic characteristics of a tall steel chimney. Part 1 Ambient response measurements, Summaries of Technical Papers of Annual Meeting, Architectural Institute of Japan, B-1, 2002. (in Japanese).

Yoshida, A., Tamura, Y., Masuda, K. and Ito, T., Dynamic characteristics of a tall steel chimney. Part 2 Evaluation of dynamic characteristics by 2DOF-RD technique and FDD, Summaries of Technical Papers of Annual Meeting, Architectural Institute of Japan, B-1, 2002. (in Japanese).

R. Brincker, L. M. Zhang and P. Anderson, Modal Identification from Ambient Response using Frequency Domain Decomposition, Proc. of the 18th IMAC, San Antonio, TX, USA, 2000, T1-1-1a.

Y. Tamura, L. M. Zhang, A. Yoshida, S. Nakata and T. Itoh, Ambient Vibration Tests and Modal Identification of Structures by FDD and 2DOF-RD Technique, Proc. of the 18th IMAC, San Antonio, TX, USA, 2000, T1-1-1b.

ASCE Standard, Minimum Design Loads for Building and Other Structures, 2000.